View metadata, citation and similar papers at core.ac.uk
brought to you by CORE
provided by University of Regensburg Publication Server

PHYSICAL REVIEW B **85**, 195426 (2012)

Localization of the phantom force induced by the tunneling current

Thorsten Wutscher, Alfred J. Weymouth,* and Franz J. Giessibl
Institute of Experimental and Applied Physics, University of Regensburg, 93040 Regensburg, Germany
(Received 9 March 2012; published 14 May 2012)

The phantom force is an apparently repulsive force, which can dominate the atomic contrast of an AFM image when a tunneling current is present. We described this effect with a simple resistive model, in which the tunneling current causes a voltage drop at the sample area underneath the probe tip. Because tunneling is a highly local process, the areal current density is quite high, which leads to an appreciable local voltage drop that in turn changes the electrostatic attraction between tip and sample. However, Si(111)-7×7 has a metallic surface state and it might be proposed that electrons should instead propagate along the surface state, as through a thin metal film on a semiconducting surface, before propagating into the bulk. In this paper, we first measure the phantom force on a sample that displays a metallic surface state [here, Si(111)-7×7] using tips with various radii. If the metallic surface state would lead to a constant electrostatic potential on the surface, we would expect a direct dependence of the phantom force with tip radius. In a second set of experiments, we study H/Si(100), a surface that does not have a metallic surface state. We conclude that a metallic surface state does not suppress the phantom force, but that the local resistance R_s has a strong effect on the magnitude of the phantom force.

DOI: 10.1103/PhysRevB.85.195426 PACS number(s): 68.37.Ps, 73.50.−h, 73.63.Rt

I. INTRODUCTION

Scanning probe microscopy (SPM) offers the possibility to determine structural and electronic properties of a surface on the atomic level.[1,2] The two most common SPM techniques are scanning tunneling microscopy (STM) and frequency-modulation atomic force microscopy (FM-AFM). With combined STM and FM-AFM, we recently observed a so-called phantom force on Si(111)-7×7.[3] When the tip is too far from the surface to allow the resolution of chemical contrast in the force channel, atomic contrast can still be observed in constant-height mode with an applied bias. The resulting images appeared similar to the tunneling current images. In our proposed model, the tunneling current is injected from the tip into a small area within a radius of ≈100 pm, the approximate atomic radius of Si. This causes an appreciable voltage drop that decreases the electrostatic attraction between tip and sample as a function of tunneling current, causing these phantom force images. However, a highly localized voltage drop leading to the phantom force effect appears to be incompatible with the existence of the metallic surface state of the Si(111)-7×7 surface.

The Si(111)-7×7 surface is described by the dimer-adatom-stacking-fault (DAS) model.[4] One unit cell of the surface consists of 12 adatoms, which have partially filled dangling bonds, forming a metallic surface state.[5] An intriguing question is how electrons propagate through the metallic surface state, which is still under discussion and we refer the reader to Refs. 6–13. A popular description is that electrons, tunneling from a STM tip onto the surface, propagate along the metallic surface state before entering the bulk. To estimate the extension of a voltage drop on a surface with and without a metallic surface state, we used finite-element analysis (FEA) software to illustrate these two cases.[14] For a surface without a metallic surface state, we modelled a silicon semiconductor sample with a constant conductivity, shown in Fig. 1(a). To mimic a surface with a metallic surface state, we added a thin metal sheet on top of the sample [Figs. 1(b)–1(d)]. The FEA was performed with increasing conductivities of the metal sheet, $\sigma_s = 10^2 \frac{\text{S}}{\text{m}}$ (b), $\sigma_s = 10^4 \frac{\text{S}}{\text{m}}$ (c), and $\sigma_s = 10^6 \frac{\text{S}}{\text{m}}$ (d), since these metal sheet conductivities cover the range of surface state conductivities noted in Ref. 10, with, e.g., $10^4 \frac{\text{S}}{\text{m}} \cdot 1$ Å corresponding to $1 \frac{\mu\text{S}}{\square}$. In each case, (a)–(d), we defined a highly localized current source on the surface. The current density was set to $\frac{1\text{ nA}}{(100\text{ pm})^2\pi} = 31 \frac{\text{GA}}{\text{m}^2}$. In Fig. 1(a), without a metal sheet, the voltage drop amounts to 230 mV and is highly focused. In Figs. 1(b)–1(d), with a metal sheet, the voltage drop shows a reduction of its amount and an increasing lateral extension for increasing conductivities of the metal sheet. As we have observed the phantom force effect on the Si(111)-7×7 surface, the question remains how the metallic surface state relates to the phantom force.

This paper gives a description of the phantom force based on our model of an attractive electrostatic force in Sec. II. Section III introduces to the equipment and methods used for the experiments. In Sec. IV we investigate whether the metallic surface state has an effect on our observations on Si(111)-7×7. If it does, we would expect a delocalized effect and thus for the observed phantom force to depend on the macroscopic tip radius R, just as the electrostatic force between a plate and a semispherical tip depends on the radius.[15,16] To evaluate this, we performed constant height images on Si(111)-7×7 to extract the ratio between the frequency shift due to the phantom force and the tunneling current ["phantom force slope," defined in Eq. (7)] and relate it to the macroscopic tip radius R, which was determined by force versus distance spectroscopy at zero effective bias. Following the conclusions from our finite-element analysis and our theory presented in Ref. 3, the phantom force is expected to occur on a surface without a metallic surface state. This has not yet been demonstrated experimentally. In Sec. V, we show the phantom force effect on a sample that does not have a metallic surface state.

 ©2012 American Physical Society

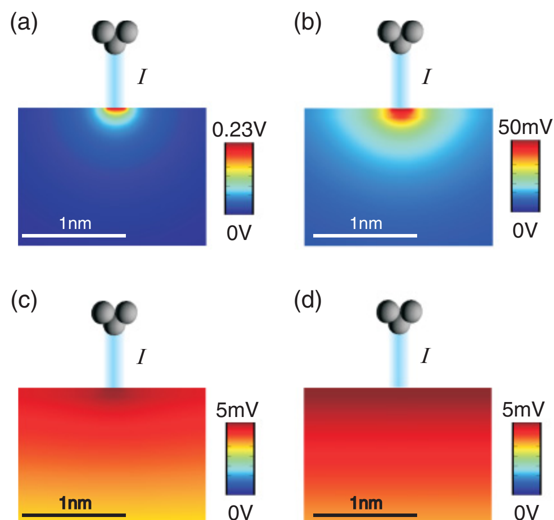

FIG. 1. (Color online) Finite-element analysis of a voltage drop in a plain bulk material (a) and a bulk material covered with a thin metal sheet on top (b)–(d) are shown. The bulk material has a constant conductivity of $\sigma_b = 10\frac{\text{S}}{\text{m}}$ [equal to the Si(111) sample used in the experiment]. In (b)–(d) the metallic surface state of Si(111)-7×7 is modelled by a metal sheet with a thickness of 100 pm. The conductivities of the metal sheet increase with $\sigma_s = 10^2\frac{\text{S}}{\text{m}}$, (b), $\sigma_s = 10^4\frac{\text{S}}{\text{m}}$, (c), to $\sigma_s = 10^6\frac{\text{S}}{\text{m}}$ in (d). Without the conductive surface layer, (a), the voltage drop amounts to 230 mV and is highly localized, while the conductive surface layer leads to a reduction and a lateral spreading of the voltage drop.

II. THEORETICAL DESCRIPTION OF THE PHANTOM FORCE

In this section, we introduce FM-AFM and describe the expected relation between the FM-AFM signal and the tunneling current in contrast to the relation between FM-AFM signal and tunneling current with a phantom force. Additionally, we mathematically derive the contribution of the tunneling current on the electrostatic force.

In FM-AFM, the forces between tip and sample cause a frequency shift Δf relative to the resonance frequency f_0 of an unperturbated cantilever.[17,18] The cantilever has a stiffness k and oscillates with a constant amplitude A at a distance z from the surface. For small amplitudes, the relation between the force F_{ts} and Δf is $\Delta f \approx \frac{f_0}{2k}k_{ts}$, where $k_{ts} = -\frac{dF_{ts}}{dz}$ is the force gradient between tip and sample.[19] For a Morse potential, which describes the chemical interaction between tip and sample atom, the force and Δf behave as shown in Fig. 2. In region I, as the tip approaches the sample, the force becomes more attractive and Δf more negative. Approaching the tip closer to the sample, attractive chemical bonds start to form and Δf decreases further. In region II, Δf starts to increase. In this paper, we focus on region I, which is the region at the onset of current. A more detailed explanation of the behavior between force and Δf is given, e.g., in Ref. 18. When performing STM, the tunneling current exponentially increases with decreasing tip-sample distance.[20] If force and current were independent, we would expect a decrease in the frequency shift as the tunneling current increases on a Δf versus I plot. However, a surprising characteristic of the phantom force is the increase of the frequency shift as the tunneling current increases when plotting Δf against I.[3]

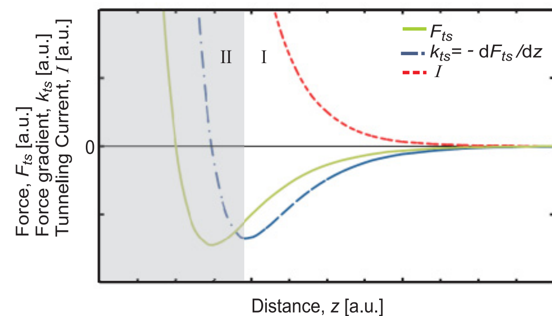

FIG. 2. (Color online) Qualitative distance dependence of the force F_{ts} according to a Morse potential, the corresponding force gradient k_{ts}, and the tunneling current I. For small cantilever amplitudes, the frequency shift Δf is proportional to k_{ts}. In region I, Δf decreases, whereas I increases. In region II, Δf starts to increase.

The phantom force can be modelled by extending the formula of the attractive electrostatic force between two metal objects by a tunneling current dependent term. Without the influence of the tunneling current we can write

$$F_{ts}^{es} = -\frac{1}{2}\frac{dC_{ts}}{dz}V^2, \qquad (1)$$

where V is the potential difference between tip and sample, and C_{ts} is the capacity of the tip-sample junction. If the tip was a flat surface A at a distance z to the sample, the derivative of capacity with distance would be given by

$$\frac{dC_{ts}}{dz} = -\epsilon_0\frac{A}{z^2}. \qquad (2)$$

The permittivity of vacuum $\epsilon_0 \approx 8.85$ pF/m can also be expressed as $\epsilon_0 \approx 8.85\ \text{pN/V}^2$. Thus, for $A = 20z^2$, a force of about 90 pN would arise for a bias of 1 V, increasing with the square of voltage.

The effective bias responsible for the electrostatic force is $V = V_{\text{bias}} - V_{\text{CPD}}$, where V_{bias} is the applied voltage and V_{CPD} is the contact potential difference between tip and sample.[21] While local changes in V_{CPD} (Ref. 22) will affect the local electrostatic attraction between tip and sample dependent upon V_{bias}, they cannot explain observations of this phantom force, for reasons discussed in Ref. 3: A local change in V_{CPD} would cause a Δf decrease in one bias (assuming the applied $|V_{\text{bias}}| > |V_{\text{CPD}}|$) and an increase in the opposite bias, whereas we observe an increase in Δf with significant bias in both bias polarities.

We thus consider the voltage V being modified by a voltage drop caused by the tunneling current passing through the sample with resistivity R_s. Therefore $V = V_{\text{bias}} - I \cdot R_s$. The electrostatic force is then

$$F_{ts}^{es} = -\frac{1}{2}\frac{dC_{ts}}{dz}\left(V_{\text{bias}}^2 - 2V_{\text{bias}}IR_s + I^2R_s^2\right) \qquad (3)$$

with an offset component proportional to V_{bias}^2, a term linear with I and a quadratic term in I. At typical experimental conditions as in our previous experiments, where $V_{\text{bias}} = 1.5$ V, $R_s = 150$ MΩ and $I = 1$ nA,[3] the quadratic term is 5% of the linear term and can be neglected (however, for very small

tip-sample distances as required for atomically resolved AFM on low-conductivity samples, this term cannot be neglected). Without the quadratic term, Eq. (3) reduces to

$$F_{ts}^{es} \approx -\frac{1}{2}\frac{dC_{ts}}{dz}\left(V_{\text{bias}}^2 - 2V_{\text{bias}} I R_s\right). \quad (4)$$

In order to determine a relation between the frequency shift Δf and the tunneling current I, we first have to calculate the contribution of this electrostatic force to the force gradient, k_{ts}^{es}. After substituting $I = I_0 e^{-\kappa z}$ into Eq. (4) and taking the derivative of F_{ts}^{es} with respect to z, Eq. (4) results in

$$k_{ts}^{es} = \frac{1}{2}\frac{d^2C_{ts}}{dz^2}V_{\text{bias}}^2 - \left(\frac{d^2C_{ts}}{dz^2} - \frac{dC_{ts}}{dz}\kappa\right)V_{\text{bias}} I R_s. \quad (5)$$

Since Δf is directly proportional to k_{ts}^{es}, assuming the small amplitude approximation, Eq. (5) can be rewritten as

$$\Delta f = \frac{f_0}{4k}\frac{d^2C_{ts}}{dz^2}V_{\text{bias}}^2 - \frac{f_0}{2k}\left(\frac{d^2C_{ts}}{dz^2} - \frac{dC_{ts}}{dz}\kappa\right)V_{\text{bias}} R_s I. \quad (6)$$

The Δf line shows a linear dependence with I with an offset that depends on capacity and bias and a slope that is linear with R_s and V_{bias}. We define, from Eq. (6), the phantom force slope as

$$\Xi := \frac{d(\Delta f)}{dI} = -\frac{f_0}{2k}\left(\frac{d^2C_{ts}}{dz^2} - \frac{dC_{ts}}{dz}\kappa\right)V_{\text{bias}} R_s, \quad (7)$$

which is usually expressed in $\frac{\text{Hz}}{\text{nA}}$. The slope is a measure of the strength of the phantom force.

III. EXPERIMENTAL METHODS AND SETUP

The experiments were performed in ultrahigh vaccum ($\approx 3 \times 10^{-10}$ Torr) and at room temperature. The images in this paper were all acquired in constant height mode. qPlus sensors ($k = 1800\frac{\text{N}}{\text{m}}$) were equipped with tungsten tips to probe the sample. The tungsten tips were prepared by common techniques like controlled collision with the sample, field emission, and explosive delamination.[23]

The Si(111)-7×7 samples used were p doped with $\rho = 6-9\ \Omega$ cm at 300 K. The surface was prepared by repeated cycles of flashes up to 1250 °C followed by cooling periods in the range of several minutes.

The n-doped Si(100) samples had a resistivity of 0.008–0.012 Ω cm at 300 K. The surface was cleaned by the same flash routine as described above. After cleaning, approximately 300 L deuterium[24] were deposited onto the surface at ≈450 °C.

A. Investigation of a potential preamplifier artifact

In the experimental setup, the bias voltage V_{bias} was applied to the tip with the sample referenced to virtual ground via a preamplifier (preamp). The preamp is attached outside vacuum and amplifies, as a current-to-voltage converter, the I signal by a factor of $10^8\frac{\text{V}}{\text{A}}$. Since the tip is oscillating, I is an alternating current (ac) with a direct current (dc) offset, where only the dc component is measured by the preamp due to its limited bandwidth. To investigate if this phantom force effect is not due to a fluctuation of the virtual ground of the preamp, we introduced a switch that allows us to either connect the sample to real ground via a direct ground connection or the virtual

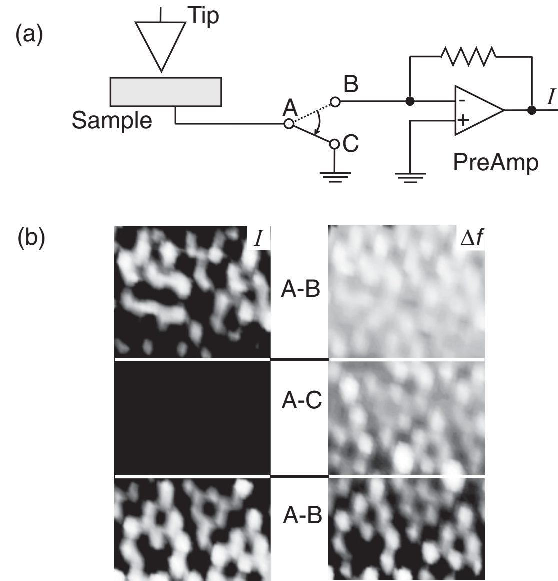

FIG. 3. (a) Schematic of the experimental setup. With an implemented switch, the preamp can be used for the I signal (switch in position A-B) or can be shorted to ground (switch in position A-C). In (b), simultaneous acquired I and Δf data in constant height mode are shown. The images were scanned from top to bottom. In the middle section the I signal was shorted to ground to check if the phantom force effect is real (i.e., caused by a voltage drop at the sample surface) or caused by a preamp artifact.

ground of the preamp, as schematically shown in Fig. 3(a). Because the operational amplifier used in the preamp has a limited gain, limited bandwidth, and a limited slew rate (in contrast to an ideal operational amplifier), the virtual ground terminal can deviate from zero, and cross coupling to the force gradient measurement might occur.

In the upper and lower section of Fig. 3(b), simultaneously recorded I and Δf data are presented in constant height mode (switch in position A-B). In the middle section of the image, the I signal from the sample was shorted to ground (switch in position A-C). Nevertheless, the phantom force effect is still present in the Δf signal, which clearly demonstrates that the phantom force is not caused by a preamp artifact, but by the current-induced local potential deviation outlined above.

IV. THE DEPENDENCE OF THE PHANTOM FORCE ON THE MACROSCOPIC TIP RADIUS ON SI(111)-7×7

In the following section, we investigate the phantom force on the Si(111)-7×7 surface. If the metallic surface state does not play a measurable role, and the phantom force is highly localized, then the macroscopic tip radius R [e.g., a large tip radius shown schematically in Fig. 4(a) versus a small tip radius shown in Fig. 4(b)] would not effect the phantom force. We would therefore not observe a dependence of the phantom force on the macroscopic tip radius R. We also discuss the results based on the description of the phantom force slope Ξ given in Eq. (7).

Figures 5(a) and 5(b) show simultaneously acquired I and Δf data of the Si(111)-7×7 surface. In Fig. 5(a) the tunneling current reaches its maximum above the adatoms. In Fig. 5(b)

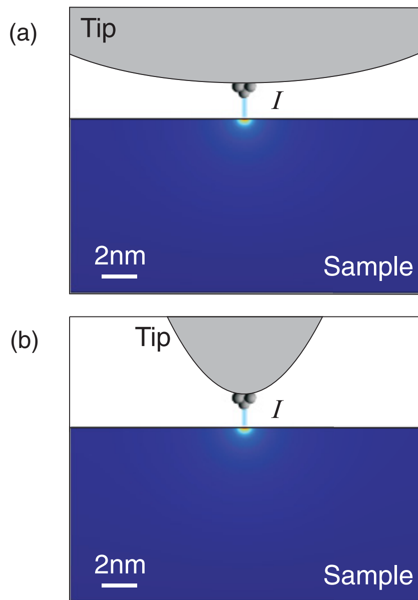

FIG. 4. (Color online) (a) Schematic of a tip with a large macroscopic radius in front of a surface with a highly localized change of the surface potential induced by the tunneling current. (b) The same situation, but with a smaller tip.

the brighter adatoms show a repulsive force contribution. The frequency shift is less negative over regions with a high tunneling current. A linear dependence between Δf and the I signal is shown in Fig. 5(c). By fitting the data we extracted a phantom force slope $\Xi = 0.73\frac{\text{Hz}}{\text{nA}}$.

The macroscopic tip can be described by its tip radius R, which we determined by fitting the long-range Δf contribution between tip and sample to a model assuming only van der Waals interaction.[25] In order to minimize the attractive

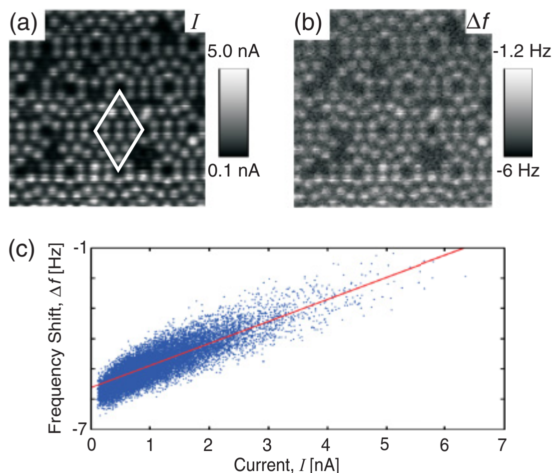

FIG. 5. (Color online) (a) Tunneling current I and (b) Δf data taken during constant height scanning. A Si(111)-7×7 unit cell is outlined by a white diamond in (a). In (b) the adatoms appear more bright, which is due to less attraction induced by the tunneling current. (c) Phantom force contribution as a linear dependence between the current and Δf data. The phantom force slope Ξ of the line is $0.73\frac{\text{Hz}}{\text{nA}}$. Images are 10 nm×10 nm, $A \approx 400$ pm, $k = 1800\frac{\text{N}}{\text{m}}$, $f_0 = 19\,130$ Hz and $V_{\text{bias}} = -1.5$ V.

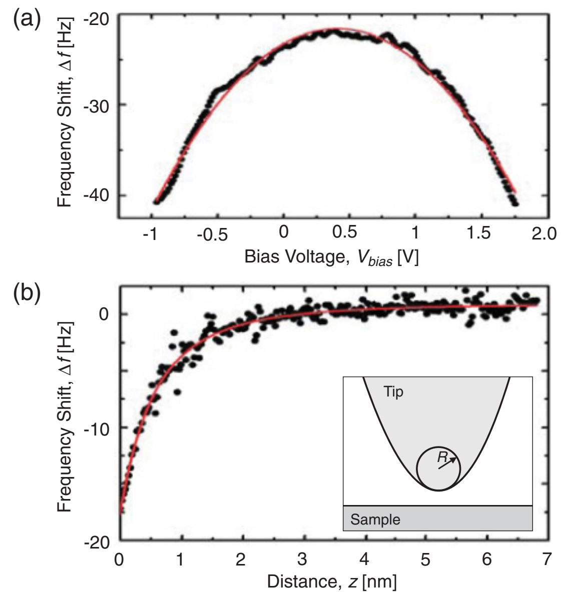

FIG. 6. (Color online) (a) Spectrum of $\Delta f(V_{\text{bias}})$ for determining the V_{CPD} between tip and sample to 0.4 V. (b) Spectrum of $\Delta f(z)$ taken at V_{CPD}. The macroscopic tip radius R was extracted by fitting the curve to a long-range van der Waals force contribution, for (b) the extracted $R = 600$ nm. The inset shows the tip radius for a parabolic tip shape.

electrostatic force, we took $\Delta f(z)$ spectra while compensating for the V_{CPD}. Before measuring the $\Delta f(V_{\text{bias}})$, we retracted the tip from the sample by 100 pm. This reduced the possibility of tip-sample collisions due to drift. The voltage corresponding to the maximum Δf value of the parabolic $\Delta f(V_{\text{bias}})$ curve is V_{CPD}.[26] In Fig. 6(a) the V_{CPD} was determined to be 0.4 V. The $\Delta f(z)$ curves were fitted to a model incorporating a parabolic tip shape [as shown in Fig. 6(b)] in accordance to Refs. 25 and 27. The fit of the $\Delta f(z)$ data in Fig. 6(b) result in $R = 600$ nm.

Figure 7 displays different phantom force slopes Ξ dependent on the respective macroscopic tip radius R. Sixteen data points, acquired with two different qPlus sensors (sensor 1: red triangles; sensor 2: blue dots), are plotted. The data points are widely spread and range from radii of 51–6775 nm.

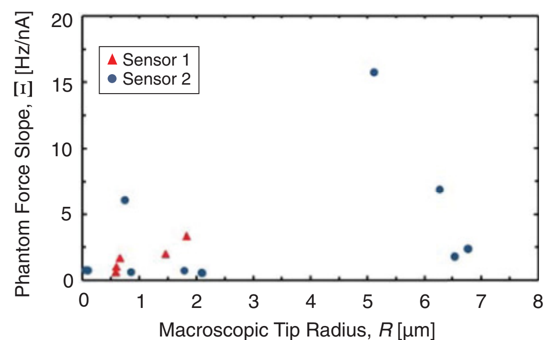

FIG. 7. (Color online) The phantom force slope Ξ in $\frac{\text{Hz}}{\text{nA}}$ characterizing the phantom force is plotted versus the macroscopic tip radii R. Two different sensors were used: sensor 1 (red triangles) and sensor 2 (blue dots). The phantom force slopes Ξ show no dependence on the macroscopic tip radii R.

The phantom force slopes vary from $0.51\frac{\mathrm{Hz}}{\mathrm{nA}}$ to $15.74\frac{\mathrm{Hz}}{\mathrm{nA}}$. In particular, slopes below $2.0\frac{\mathrm{Hz}}{\mathrm{nA}}$ can be observed for a wide range of macroscopic tip radii R. We observe no dependence between the phantom force slope and the macroscopic tip radius. This supports our hypothesis of a highly local voltage drop, and suggests that the metallic surface state does not play a role.

The spread in our measurements of Fig. 7 can be discussed with the aid of Eq. (7), $\Xi = -\frac{f_0}{2k}(\frac{d^2C_{ts}}{dz^2} - \frac{dC_{ts}}{dz}\kappa)V_{\text{bias}}R_s$. We turn now to the factors $-\frac{f_0}{2k}(\frac{d^2C_{ts}}{dz^2} - \frac{dC_{ts}}{dz}\kappa)$ and R_s in detail, as V_{bias} was constant for these measurements.

The factor $-\frac{f_0}{2k}(\frac{d^2C_{ts}}{dz^2} - \frac{dC_{ts}}{dz}\kappa)$ can be calculated, assuming a model of the electrostatic force F_{ts}^{es} of a conical tip (half angle θ) in front of a metallic surface as described by Hudlet *et al.*[16] This would be applicable, if the tip and sample surfaces could be modelled by a constant potential. Calculations for realistic $R = 5$ nm and $\theta = 70^\circ$, at conditions summarized in Ref. 28, lead to unrealistic values of $\Xi = 68\frac{\mathrm{Hz}}{\mathrm{nA}}$, much larger than $2.8\frac{\mathrm{Hz}}{\mathrm{nA}}$, the experimentally determined average Ξ of the values shown in Fig. 7. We propose that this phantom force effect is highly localized. Instead of being described by the macroscopic tip shape, it would be better described by a model of the nanoscopic tip cluster. Assuming a plate capacitor with $C = \epsilon_0\frac{A}{z}$, we can calculate the phantom force slope using Eq. (7) and the following parameters: $f_0 = 20$ kHz, $k = 1800$ N/m, $\kappa = 2$ Å^{-1}, $R_s = 150$ MΩ with an applied bias $V_{\text{bias}} = -1.5$ V, at a distance $z = 4.4$ Å and a capacitive area $A = (1\ \text{nm})^2$. This yields a slope $\Xi = 2.8\frac{\mathrm{Hz}}{\mathrm{nA}}$, equivalent to the experimental average of $2.8\frac{\mathrm{Hz}}{\mathrm{nA}}$. While a parallel plate capacitor might be an oversimplification at this length scale, local capacitive interaction (that is, a parabolic dependence of the force with respect to an applied bias voltage) between tip and sample has been reported at the atomic scale.[29]

Concerning the factor R_s, we observed in Ref. 3 that the higher the sample resistivity the higher the slope Ξ. In our case, the data points with higher Ξ were collected on areas with an increased number of defects on the Si(111)-7×7 surface. The dependence between Ξ and the defect density on the Si(111)-7×7 surface was investigated and is shown in Fig. 8. For low defect densities, Ξ seems to be low in contrast to higher defect densities with an increased Ξ. But, since the tip shape and R_s changed for each data point, the dependence between phantom force slopes and the defect densities is not conclusive and has to be investigated in more detail.

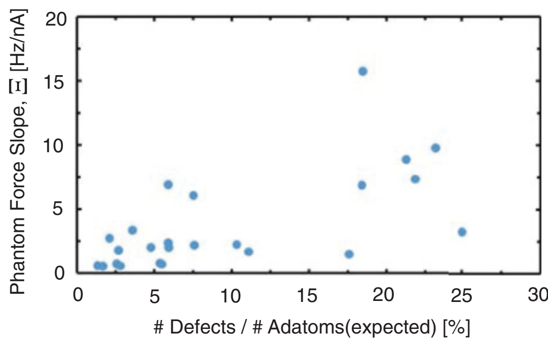

FIG. 8. (Color online) Phantom force slopes Ξ plotted versus the defect density on the Si(111)-7×7 surface. The phantom force slopes Ξ seem small for less defects on the Si(111)-7×7 and more defects point to increased Ξ.

V. THE PHANTOM FORCE ON THE HYDROGENATED SI(100) SURFACE

In this section, we present measurements on the H/Si(100) surface. Exposing Si(100) to hydrogen saturates the unsaturated dangling bonds.[30] The electronic states of the hydrogenated dimers have been shown to be outside the band gap of bulk Si, meaning that in contrast to Si(111)-7×7, the surface does not have a metallic surface state.[31]

In Fig. 9(a), a tunneling current between tip and sample, which leads to the phantom force effect, is schematized. Figures 9(b) and 9(c) show simultaneous Δf and I data collected at constant height with an applied bias voltage of 1.5 V. The dimer rows can be seen running from upper left to lower right. The low contrast is due to our choice of a relatively large

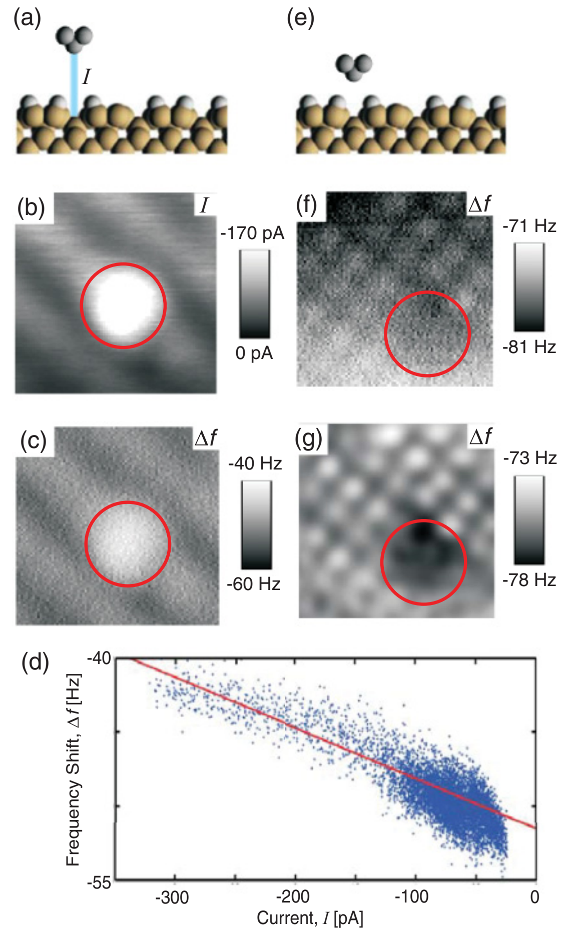

FIG. 9. (Color online) (a) At tip-sample distances characteristic for STM and with a tunneling current, the phantom force effect can be observed. Simultaneous acquired I and Δf data with atomic contrast are shown in (b) and (c) for $V_{\text{bias}} = 1.5$ V. In (d), the relation between Δf and I data is plotted. Data points with increased I data, as the defect outlined in red, show a stronger decrease (less attraction) of the Δf values. However, at close tip-sample distances, (e), and low bias, in this case 200 mV, the defect appears darker (more attractive), (f). Image (g) shows (f) with low-pass filtering and plane substraction applied for clarity. Images are 2 nm × 2 nm, $A =$ 100 pm, $k = 1800\frac{\mathrm{N}}{\mathrm{m}}$, $f_0 = 19\,131$ Hz.

imaging distance to prevent excessive tunneling currents when scanning over the defect area, circled in red. The feature circled in red is most likely a dangling bond, which we would expect to observe in Δf data as darker (more attractive). However, due to the increase of the tunneling current over it, the phantom force effect causes an increase in Δf that makes it appear brighter. To investigate the relationship between Δf and I, we plotted in Fig. 9(d) the Δf information of each single pixel in image (c) versus the corresponding pixel of the I information in (b). For positive applied bias voltages, the I signal is negative. The relation between Δf and I data results in $\Xi = -34\frac{\text{Hz}}{\text{nA}}$, if we assume a linear relation as described in Eq. (6).

In Fig. 9(e), the bias voltage is decreased to 200 mV and in order to resolve atomic contrast, the tip must be approached to the surface, similar to our previous observations of the phantom force.[3] The attractive interaction in the presence of the dangling bond is clearly observed in Δf data collected at low bias, as shown in Fig. 9(f). Figure 9(g) is a low-pass filtered and plane substracted image from (f) to show the dangling bond with better contrast. We demonstrated that the phantom force does not depend on the presence of a metallic surface state and still appears on a sample system as H/Si(100) without a metallic surface state.

It is useful to contrast the phantom force with a phenomenon observed on semiconductors without a metallic surface state, known as tip-induced band bending (TIBB). Without a metallic surface, the electric field of the tip penetrates into the surface and part of the voltage between tip and sample drops in the sample itself.[32] In contrast to the phantom force, TIBB can have a lateral extension in the range of tens of nm and is strongly dependent on the macroscopic tip radius.[33] TIBB does not require a current; it is a voltage drop within the sample that itself changes the tunneling current. The phantom force, on the other hand, is a current-induced drop of voltage within the sample. These two phenomena manifest themselves differently upon the attractive electrostatic force: the voltage drop induced by TIBB is not current dependent and the attractive electrostatic force should be constant in a small scan area, whereas the phantom force can explain atomic-scale variations in the electrostatic force that vary with current. It should be noted as well that STM investigations of TIBB also indicated current-related effects, possibly related to the phantom force.[34]

VI. SUMMARY AND OUTLOOK

Section III introduces to the equipment and methods used for the experiments. It was shown that the phantom force is not an effect of the tunneling current amplifier.

In Sec. IV, we investigated the influence of a metallic surface state on the phantom force. The experimental observation of the phantom force slope Ξ shows no dependence on the macroscopic tip radius R. This infers a highly localized voltage drop and we concluded that the metallic surface state does not play a role in the phantom force effect. Finally, in Sec. V, we showed that the phantom force is present on a sample system without a metallic surface state, which had not explicitly been demonstrated experimentally.

For a future project we suggest low-temperature measurements to investigate the dependence of the phantom force on the defect density on Si(111)-7×7. In this experiment, the tip would be more stable and a controlled exposure of a distinct spot on the surface to, e.g., oxygen could clarify the dependence between phantom force and sample resistivity.

ACKNOWLEDGMENTS

The authors thank the German Science Foundation (DFG, Sonderforschungsbereich 689) for financial support, and J. Welker, M. Emmrich, E. Wutscher, and F. Pielmeier for helpful discussions.

*jay.weymouth@physik.uni-r.de

[1] M. Ternes, C. Gonzalez, C. P. Lutz, P. Hapala, F. J. Giessibl, P. Jelinek, and A. J. Heinrich, Phys. Rev. Lett. **106**, 016802 (2011).
[2] Y. Sun, H. Mortensen, S. Schär, A. S. Lucier, Y. Miyahara, P. Grütter, and W. Hofer, Phys. Rev. B **71**, 193407 (2005).
[3] A. J. Weymouth, T. Wutscher, J. Welker, T. Hofmann, and F. J. Giessibl, Phys. Rev. Lett. **106**, 226801 (2011).
[4] K. Takayanagi, Y. Tanishiro, and S. Takahashi, J. Vac. Sci. Technol. A **3**, 1502 (1985).
[5] M. Mauerer, I. L. Shumay, W. Berthold, and U. Höfer, Phys. Rev. B **73**, 245305 (2006).
[6] B. N. J. Persson, Phys. Rev. B **34**, 5916 (1986).
[7] S. Hasegawa and S. Ino, Phys. Rev. Lett. **68**, 1192 (1992).
[8] Y. Hasegawa, I.-W. Lyo, and Ph. Avouris, Appl. Surf. Sci. **76-77**, 347 (1994).
[9] S. Heike, S. Watanabe, Y. Wada, and T. Hashizume, Phys. Rev. Lett. **81**, 890 (1998).
[10] M. D'angelo, K. Takase, N. Miyata, T. Hirahara, S. Hasegawa, A. Nishide, M. Ogawa, and I. Matsuda, Phys. Rev. B **79**, 035318 (2009).
[11] T. Tanikawa, K. Yoo, I. Matsuda, S. Hasegawa, and Y. Hasegawa, Phys. Rev. B **68**, 113303 (2003).
[12] K. Yoo and H. H. Weitering, Phys. Rev. B **65**, 115424 (2002).
[13] J. W. Wells, J. F. Kallehauge, T. M. Hansen, and Ph. Hofmann, Phys. Rev. Lett. **97**, 206803 (2006).
[14] [http://www.comsol.com], version 4.2 (2011).
[15] L. Olsson, N. Lin, V. Yakimov, and R. Erlandsson, J. Appl. Phys. **84**, 8 (1998).
[16] S. Hudlet, M. Saint-Jean, C. Guthmann, and J. Berger, Eur. Phys. J. B **25**, 5 (1998).
[17] T. R. Albrecht, P. Grütter, D. Horne, and D. Rugar, J. Appl. Phys. **69**, 668 (1991).
[18] F. J. Giessibl, Rev. Mod. Phys. **75**, 949 (2003).
[19] F. J. Giessibl, Appl. Phys. Lett. **78**, 123 (2001).
[20] G. Binnig, H. Rohrer, Ch. Gerber, and E. Weibel, Phys. Rev. Lett. **50**, 120 (1983).
[21] M. Nonnenmacher, M. P. O'Boyle, and H. K. Wickramasinghe, Appl. Phys. Lett. **58**, 2921 (1991).
[22] S. Sadewasser, P. Jelinek, C. K. Fang, O. Custance, Y. Yamada, Y. Sugimoto, M. Abe, and S. Morita, Phys. Rev. Lett. **103**, 266103 (2009).
[23] T. Hofmann, J. Welker, and F. J. Giessibl, J. Vac. Sci. Technol. B **28**, C4E28 (2010).
[24] The Si(100) surface was saturated with deuterium, which for purposes of this study behaves as hydrogen.

[25] H. Hölscher, U. D. Schwarz, and R. Wiesendanger, Appl. Surf. Sci. **140**, 344 (1999).
[26] M. Guggisberg, M. Bammerlin, Ch. Loppacher, O. Pfeiffer, A. Abdurixit, V. Barwich, R. Bennewitz, A. Baratoff, E. Meyer, and H.-J. Güntherodt, Phys. Rev. B **61**, 11151 (2000).
[27] F. J. Giessibl, Phys. Rev. B **56**, 16010 (1997).
[28] Further conditions for the calculation of Ξ were: $f_0 = 20\,000$ Hz, $k = 1800\,\frac{\mathrm{N}}{\mathrm{m}}$, $\kappa = 2$ Å^{-1}, $L_{\mathrm{tip}} = 300\ \mu$m, $z = 500$ pm, $V_{\mathrm{bias}} = -1.5$ V, $R_s = 150$ MΩ.
[29] L. Gross, F. Mohn, P. Liljeroth, J. Repp, F. J. Giessibl, and G. Meyer, Science **324**, 1428 (2009).
[30] J. J. Boland, Phys. Rev. Lett. **65**, 3325 (1990).
[31] H. Raza, Phys. Rev. B **76**, 045308 (2007).
[32] R. M. Feenstra, Y. Dong, M. P. Semtsiv, and W. T. Masselink, Nanotechnology **18**, 044015 (2007).
[33] R. M. Feenstra, J. Vac. Sci. Technol. B **21**, 2080 (2003).
[34] R. M. Feenstra, G. Meyer, and K. H. Rieder, Phys. Rev. B **69**, 081309 (2004).